DOI: 10.1002/ejic.200700202

Crystal Structure and Surface Photovoltage Properties of Mn^{II} Coordination Supramolecules

Li-Ping Sun,[a] Shu-Yun Niu,*[a] Jing Jin,[a] and Li Zhang[a]

Keywords: Manganese / Hydrogen bonds / Surface photovoltage spectroscopy

Three Mn^{II} coordination supramolecular complexes $[Mn(pdc)(H_2O)]_n$ **1**, $\{[Mn(pdc)(phen)(H_2O)]\cdot 3H_2O\}_n$ **2**, and $\{[Mn(cyan)_2(H_2O)_4]\cdot 2HCl\cdot 2(Hcyan)\}$ **3** (H_2pdc = pyridine-2,3-dicarboxylic acid, Hcyan = cyanuric acid, phen = 1,10-phenanthroline) were hydrothermally synthesized and their structures determined by single-crystal X-ray diffraction. The pdc group in complex **1** bridges the Mn^{II} ions to form an infinite 3D structure. In complex **2**, the Mn^{II} ion is bridged to a 1D infinite chain by pdc groups and the chain is further connected to a 2D structure by hydrogen bonds. The 3D structure of complex **3** is formed by hydrogen bonds and O···Cl weak interactions. Surface photovoltage spectroscopy (SPS) of complexes **1**–**3** indicate that they all possess positive SPV response in the range of 300–800 nm and show *p*-type semiconductor characteristic. The intensities of the SPV responses are obviously different, and this can mainly be attributed to the differences in their structures. Field-induced surface photovoltage spectroscopy (FISPS) of complexes **1**–**3** confirms their *p*-type semiconductor characteristic.

(© Wiley-VCH Verlag GmbH & Co. KGaA, 69451 Weinheim, Germany, 2007)

Introduction

In recent years, the most attractive areas of research in the fields of crystal engineering and supramolecular chemistry have been aimed at creating a wide range of purpose materials with specific structures and useful properties, such as electronic, magnetic, optical, and catalytic properties.[1,2] In inorganic coordination polymers, the choice of metal–ligand combination is the main factor controlling both the supramolecular topology and dimensionality, but other factors such as hydrogen-bonding, $\pi\rightarrow\pi^*$ interactions, and metal–metal interactions can also greatly influence the crystal structure and its dimensionality.[3,4] Owing to the particularity and variety of electronic configurations possible for manganese ions, manganese coordination complexes have attracted great attention in the domain of coordination chemistry all along, though the research of Mn^{n+} coordination complexes have gone across hundreds of years. Manganese complexes play an important role in some biological redox systems owing to the various oxidation states of the manganese ion;[5,6] the water oxidizing complex of photosystem II [PS (II)] involves manganese ions in various combinations of oxidation states, including Mn^{II}, Mn^{III}, and Mn^{IV}.[7,8] It is well-known that the electronic arrangement of the six-coordinate Mn^{II} (d^5) ion can take the high-spin (HS) and low-spin (LS) states depending on the different ligand field. The spin conversion between HS and LS probably accompanies magnetic behaviors. When Mn^{II} ion takes HS, there are more unpaired electrons, which easily leads to the behavior of paramagnetism, antiferromagnetism, and ferromagnetism.[9,10] When the Mn^{II} ion takes LS, various transitions will occur, which makes the corresponding complexes appear to have photoelectric and optical properties. In addition, Mn^{II} complexes coordinated by a carboxylic group have some potential application in human pharmaceuticals.[11] At present, research on the properties of Mn^{II} coordination complexes is mainly focused on magnetism.[12–14] Research into photoelectric properties is mainly involved in the coordination complexes which depend on phthalocyanine and porphyrin as ligands. There are few reports on the photoelectric properties of coordination polymers.[15–17] Surface photovoltage spectroscopy (SPS) is an effective technique that can be used to investigate the photophysics of the excited states and the surface charge behavior of the sample. This technique provides information about the properties of the sample surface layer (several atomic layers), and it has a very high sensitivity. The sensitivity of this method is about 10^8 $q\,cm^{-2}$, or about one elementary charge per 10^7 surface atoms, which exceeds that of conventional spectroscopy such as XPS and Auger spectroscopy by many orders of magnitude. Moreover, the SPV method is a contactless and nondestructive technique. This technique has been used to investigate the photoelectric processes such as charge transfer and photocatalysis.[18,19] On the basis of the principle of SPS, Wang and coworkers developed a field-induced surface photovoltage spectroscopy (FISPS) technique,[20,21] which can demon-

[a] School of Chemistry and Chemical Engineering, Liaoning Normal University
Dalian 116029, P. R. China
E-mail: syniu@sohu.com

Supporting information for this article is available on the WWW under http://www.eurjic.org or from the author.

 © 2007 Wiley-VCH Verlag GmbH & Co. KGaA, Weinheim

strate the photoelectric properties of semiconductors under the effect of an external electric field. In this paper we report the synthesis, structure, and properties of three Mn^{II} coordination supramolecules. Meanwhile we discuss the influence of the different structures on the photoelectric properties.

Results and Discussion

$[Mn(pdc)(H_2O)]_n$ (1)

Single-crystal X-ray diffraction analysis reveals that complex **1** possesses a 3D infinite structure and its building unit is [Mn(pdc)(H_2O)] (Figure 1a). The Mn^{II} ion is six-coordinate with an NO_5 donor set in the distorted octahedron environment. One O atom and one N atom are from the same pdc group, the other four O atoms are from three different pdc ligands and one coordinated water molecule (Figure 1b). The equatorial plane is defined by the O1, O2, O3, and O5 atoms with the O4 and N1 atoms occupying the apical positions. The bond lengths of Mn–O range from 2.1464(16) to 2.2436(18) Å and the bond length of Mn–N is 2.287(2) Å. In the crystal, the pdc group plays a bridging role. The two β-carboxylic O atoms (O2, O3) bridge equivalent Mn^{II} ions and the Mn^{II} ion is connected to a 1D infinite chain along the *a* axis. Along the *c* axis, the two α-carboxylic O atoms (O1, O5) separately coordinate to two equivalent Mn^{II} ions. The Mn^{II} ions are also connected to a 1D infinite structure. Then, complex **1** is connected to a regular 2D structure in the *ac* plane (Figure 2). Moreover, along the *b* axis, the α-carboxylic O atom (O1) together with the pyridine N atom chelate to one Mn^{II} ion, the β-carboxylic O atom (O2) coordinates to the other equivalent Mn^{II} ion, then the Mn^{II} ions are also linked to a 1D infinite chain. It can be seen that the *ab* plane is also a regular 2D web structure (Figure 3). Complex **1** is therefore webbed to a 3D infinite structure (Figure 4).

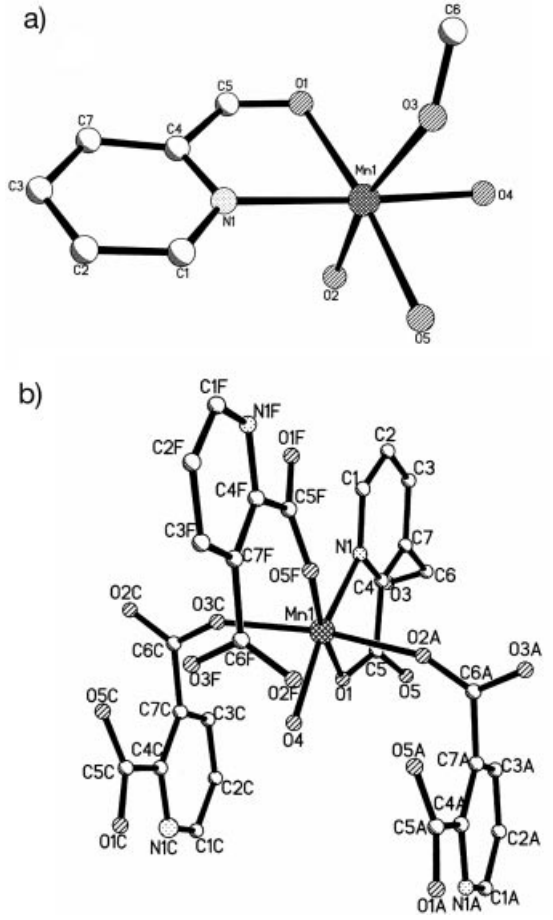

Figure 1. a) The asymmetry unit of complex **1**. b) The coordination environment of the Mn^{II} ion in complex **1**.

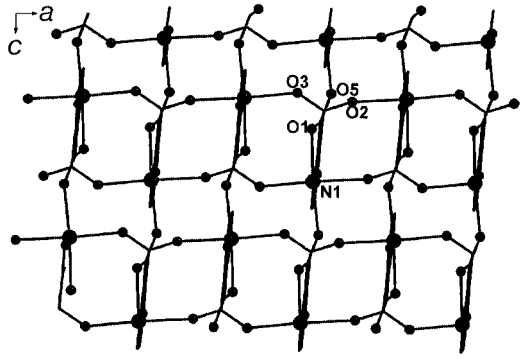

Figure 2. The 2D structure of the *ac* plane in complex **1**.

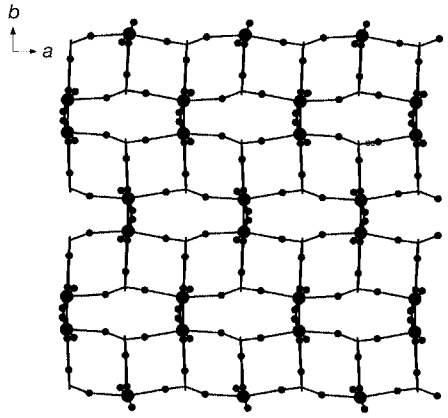

Figure 3. The 2D structure of the *ab* plane in complex **1**.

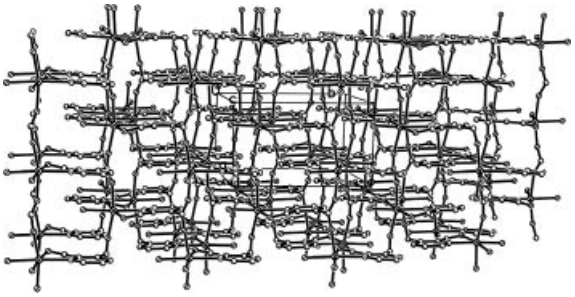

Figure 4. The 3D structure of complex **1**.

 © 2007 Wiley-VCH Verlag GmbH & Co. KGaA, Weinheim

{[Mn(pdc) (phen)(H_2O)]·3H_2O}$_n$ (2)

Single-crystal X-ray diffraction analysis reveals that complex **2** possesses a 2D infinite structure and its building unit is {[Mn(pdc)(phen)(H_2O)]·3H_2O}. The Mn^{II} ion is six-coordinate by the N_3O_3 donor (N1, N2, N3, O1, O3, and O4) set in a distorted octahedron. The equatorial plane is defined by the N1 and N2 atoms from one phen molecule and the O3 and O4 atoms from two different pdc groups. The O1 and N3 atoms are separated from the coordinated water molecules and the pdc group occupies the apical position. The bond lengths of Mn–N range from 2.2718(16) to 2.3149(15) Å and the bond lengths of Mn–O are from 2.0963(13) to 2.1710(3) Å. The pdc group plays a bridging role: its two carboxylic groups adopt a monodentate coordination mode, one together with the pyridine N atom coordinates to one Mn^{II} ion, the other coordinates to a second equivalent Mn^{II} ion. Then, the Mn^{II} ions are linked to a 1D infinite chain along the *b* axis (Figure 5). Two 1D infinite chains are connected to a 1D double chain through the hydrogen bond [O1–H···O2, 2.835(2) Å], which from the coordinated water molecule and uncoordinated carboxylic O atom (Figure 6). Between the different 1D double chains, there are two styles of O–H···O hydrogen bonds. They are the interactions between the lattice water molecules and the uncoordinated carboxylic O atoms [O6–H···O5, 2.854(3) Å, O7–H···O5, 2.833(3) Å] as well as lattice water molecules [O6–H···O8, 2.758(3) Å, O8–H···O7, 2.794(3) Å]. These hydrogen bonds link the multi 1D double chains to form an infinite structure along the *a* axis. Therefore, complex **2** is linked to a 2D irregular structure by hydrogen bonds (Figure 7).

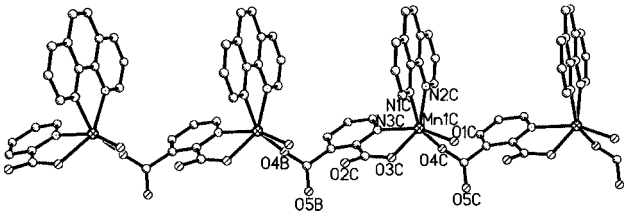

Figure 5. The 1D chain structure of complex **2**.

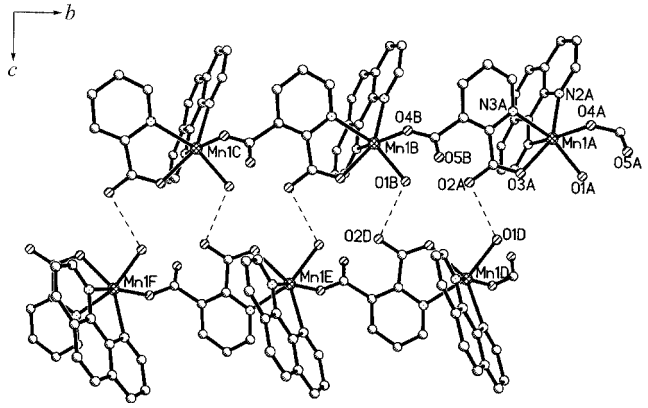

Figure 6. The 1D double chain structure of complex **2**. Dotted lines are hydrogen bonds.

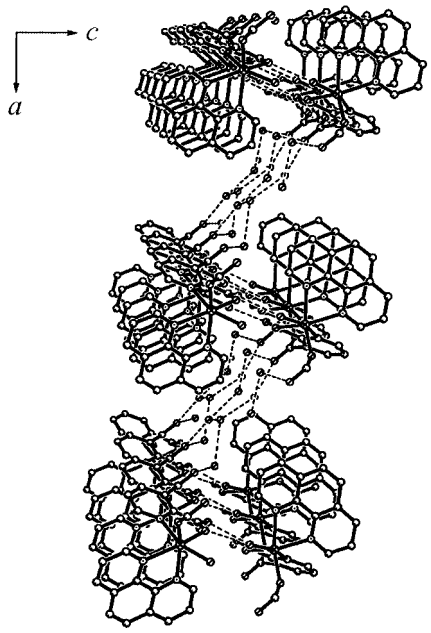

Figure 7. The 2D structure of complex **2**. Dotted lines are hydrogen bonds.

{[Mn(cyan)$_2$(H_2O)$_4$]·2HCl·2(Hcyan)} (3)

Complex **3** is a mononuclear coordination complex. The Mn^{II} ion is six-coordinate with an N_2O_4 donor set in the better octahedron environment (Figure 8). Four O atoms (O6, O6A, O3, and O3A) are from four different coordinated water molecules and they comprise the equatorial plane. The bond lengths of Mn1–O3 and Mn1–O6 are 2.228(4) and 2.238(3) Å, respectively. The O6–Mn1–O6A and O3–Mn1–O3A bond angles are all 180°. The O3–Mn1–O6 and O3A–Mn1–O6 bond angles are 95.32(14)° and 84.68(14)°, respectively. The two N atoms (N1, N1A) are from two different cyan groups and they occupy the apical positions of the octahedron. The Mn1–N bond length of 2.261(4) Å and N1–Mn1–N1A bond angles of 180° means that the coordination environment of Mn^{II} ion is a better octahedron. The free chloride ion is from the $MnCl_2$ reagent. The hydrogen ion comes from the coordinated Hcyan group. The N atom of the Hcyan group coordinates to the Mn^{II} ion, simultaneously, the N–H bond breaks, the corresponding hydrogen ion dissociates itself from the N–H

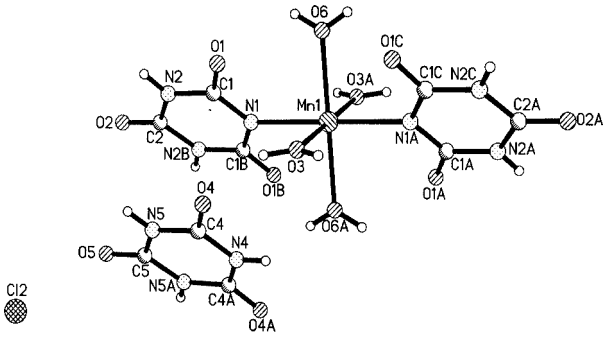

Figure 8. The molecule structure of complex **3**.

 © 2007 Wiley-VCH Verlag GmbH & Co. KGaA, Weinheim

bond to the solution and they exactly take on the action of balancing the charge. In the crystal, there are two styles of O–H···O and O–H···N hydrogen bonds. The former is from one coordinated water molecule and a carbonyl O atom of the free Hcyan, [O3–H···O4, 2.771(3) Å], the latter is from the other coordinated water molecule and the N atom of the free Hcyan group [O6–H···N4, 2.920(4) Å]. The two styles of intermolecular hydrogen bonds link the molecule to form an infinite 1D structure along the *c* axis. In addition, there are two kinds of O···Cl weak interactions between the chlorine ion and the carbonyl O atom of the coordinated cyan group (O2···Cl, 2.867 Å) as well as the carbonyl O atom of the free Hcyan group (O5···Cl, 2.893 Å). The O···Cl weak interactions also link the molecule to form a 1D infinite structure along the *b* axis. So complex **3** is linked to a 2D regular structure at the *bc* plane (Figure 9). Moreover, the weak interactions between the free chlorine ions and the coordinated water molecules (O6···Cl, 2.949 Å; O3···Cl, 2.819 Å) as well as the carbonyl O atom of the coordinated cyan group (O1···Cl, 2.906 Å) link complex **3** to form a 1D infinite structure along the *a* axis. When projecting along the *c* axis, the *ab* plane is also a regular 2D layer (Figure 10). So complex **3** is connected to a 3D structure by hydrogen bonds and a O···Cl weak interaction (Figure 11).

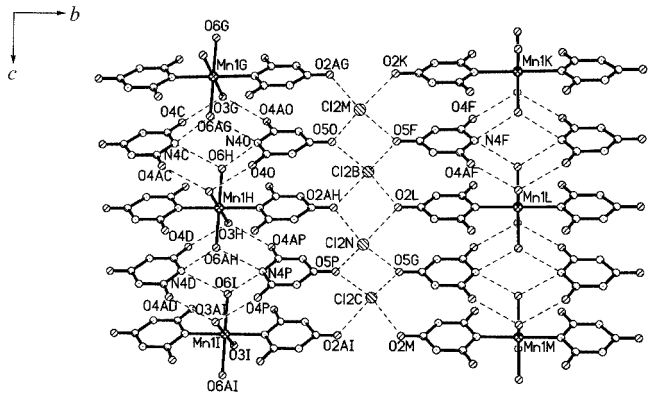

Figure 9. The 2D hydrogen-bonding structure of the *bc* plane in complex **3**. Dotted lines are hydrogen bonds.

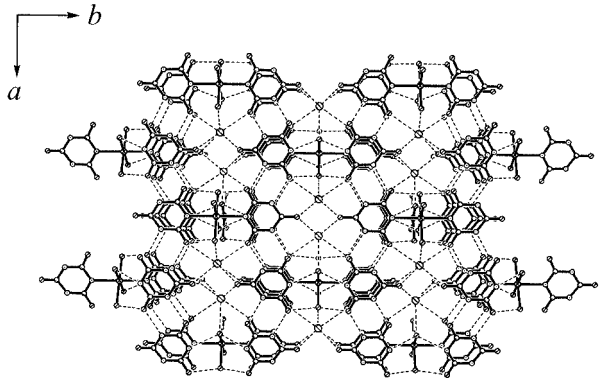

Figure 10. The 2D hydrogen-bonding structure of the *ab* plane in complex **3**. Dotted lines are hydrogen bonds.

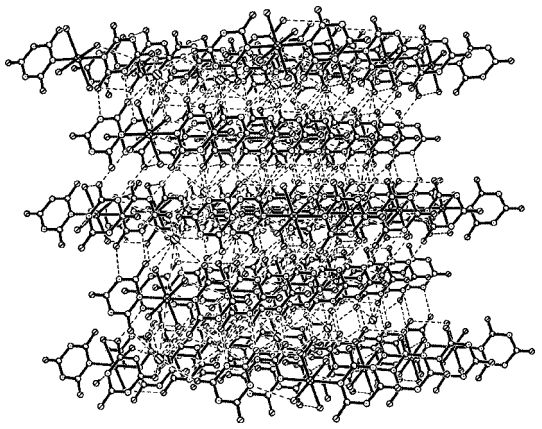

Figure 11. The 3D hydrogen-bonding structure of complex **3**. Dotted lines are hydrogen bonds.

SPS of Complexes 1–3

The emergence of the surface photovoltage (SPV) response band indicate that when the surface of the solid sample is illuminated, the electron-hole pairs separate under a built-in field, resulting in a change in the surface potential barrier, which produces the photoelectric behavior. The detected signal by SPS is equivalent to the change in the surface potential barrier on illumination (δV_s), which is given by the equation: $\delta V_s = V_s' - V_s^o$, where V_s' and V_s^o are the surface potential barriers before and after illumination, respectively. As far as band-to-band transitions are concerned, a positive response in SPV ($\delta V_s > 0$) means that the sample is characterized as a *p*-type semiconductor, whereas a negative response means that the sample is an *n*-type semiconductor. The magnitude of the surface potential barrier depends on the numbers of surface net charge. Figures 12, 13, and 14 show the SPS spectra of complexes **1**–**3**, respectively. They all appear as positive SPV response bands between 300 and 800 nm. Thereinto, the signal detected by SPS at 300–500 nm is a wide peak. The signal is actually the result of overlap of several SPV response bands. To make the assignment of each SPV response band clear, we separated them by the Origin 7.0 program. Then, complexes **1** and **3** present two positive SPV responses and complex **2** appears as three positive SPV responses in the range 300–800 nm, which indicates that they all possess *p*-type semiconductor characteristics. In complex **1**, the response at λ_{max} = 349 nm is attributed to the $\pi \rightarrow \pi^*$ transition of the ligands and the response at λ_{max} = 403 nm is assigned to the LMCT (from ligand-to-metal charge transfer) transition. At 600–800 nm, some very weak and splitting peaks appear, this phenomenon is associated with the weak crystal-field coordination environment of the Mn^{II} ion. In the six-coordinate atoms of the Mn^{II} ion, there are one N atom and five O atoms. The four O atoms are from four carboxylic groups and one O atom is from one coordination water molecule. According to the spectra chemical series (–COO $<$ H_2O $<$ N complexes), the Mn^{II} ion (d^5) in complex **1** can be regarded as lying among the weak crystal field. So the $d \rightarrow d^*$ transition is forbidden. However, the microenvi-

 © 2007 Wiley-VCH Verlag GmbH & Co. KGaA, Weinheim

ronment of the Mn^{II} ion is not a strict octahedron, and there still appears to be weak splitting SPV response bands at 600–800 nm.

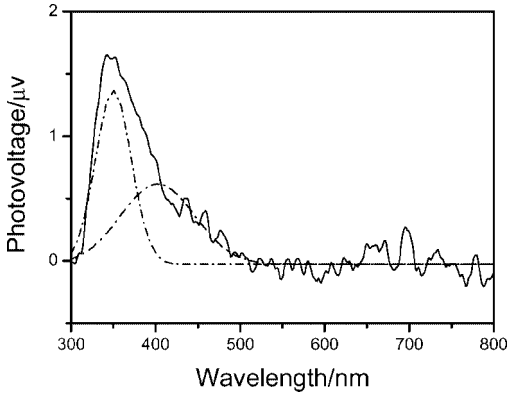

Figure 12. The SPS of complex **1**. Dotted lines are treated peak.

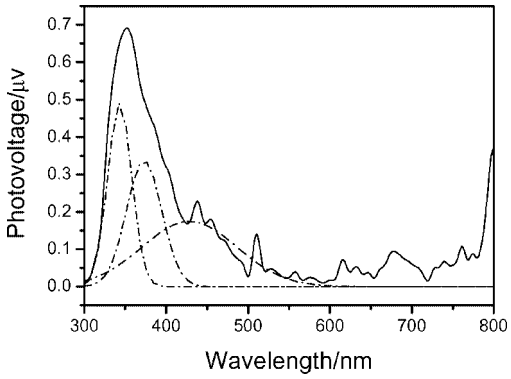

Figure 13. The SPS of complex **2**. Dotted lines are treated peak.

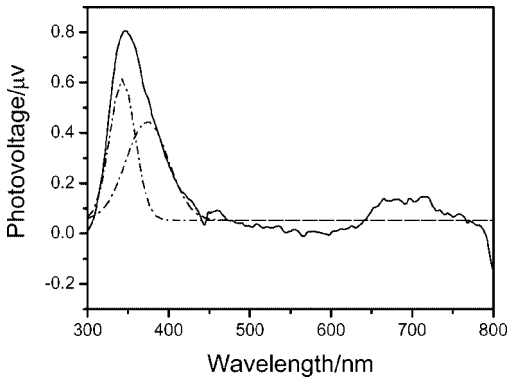

Figure 14. The SPS of complex **3**. Dotted lines are treated peak.

In complex **2**, there are three SPV responses in the range 300–800 nm. The SPV response at λ_{max} = 349 nm is assigned to the π→π* transition of the ligand and the response at λ_{max} = 370 nm is attributed to the LMCT transition. The response at λ_{max} = 429 nm can be assigned to the d→d* transition ($^2T_2 \rightarrow {}^2A_2,{}^2T_2$) of the Mn^{II} ion. In contrast with complex **1**, complex **2** has another SPV response band (λ_{max} = 429 nm) that is caused by a d→d* transition, and the energy of this SPV band is very high. This can be attributed to the crystal field of the Mn^{II} ion in complex **2**, which is different than that in complex **1**. The coordination atoms for the Mn^{II} ion in complex **2** are three N atoms and three O atoms. So it can be regarded that the crystal field of the Mn^{II} ion in complex **2** is stronger than that of in complex **1**; the d→d* transition $^2T_2 \rightarrow {}^2A_2,{}^2T_2$ can take place. The $^2T_2 \rightarrow {}^4T_1$ transition is forbidden. So only one SPV response band (λ_{max} = 429 nm) is caused by a d→d* ($^2T_2 \rightarrow {}^2A_2,{}^2T_2$) transition. The weak and splitting SPV response band at 600–800 nm is attributed to the forbidden d→d* transition ($^2T_2 \rightarrow {}^4T_1$), owing to the microenvironment of the Mn^{II} ion not being a strict octahedron.

In complex **3**, there are two positive SPV responses at 300–800 nm. The response at λ_{max} = 340 nm is attributed to the π→π* transition of the ligand, and the response at λ_{max} = 376 nm is assigned to the LMCT transition. Analogous with complex **1**, in the coordinated atoms with the Mn^{II} ion, there are two N atoms from two cyan groups and four O atoms from four coordinated water molecules. The Mn^{II} ion can be regarded as lying among a weak crystal field. The d→d* transition is forbidden. The microenvironment of the Mn^{II} ion is not a strict octahedron and a weak SPV response band at 600–800 nm appears.

Comparing the SPV responses of complexes **1**–**3** at 300–500 nm (Figure 15), it can be seen that the SPV intensity of complex **1** is larger than that of complexes **2** and **3**. The differences in their intensities are maybe mainly due to the differences in their structures. Complex **1** is a 3D infinite coordination polymer. In the crystal, the 3D structure is completely formed by the coordination bonds and it can supply more transmission passages for the electrons and holes. That means that more electrons diffuse to the surface, which leads to an increase in the SPV intensity. Moreover, the 2D plane made from the *ab* and *bc* planes in complex **1** is a regular structure, and it is very favorable for the transmission of electrons and holes. Although complex **2** possesses a 2D infinite structure, the 2D structure is an irregular space structure. The irregular space structure in transferring electrons and holes is smaller than the regular structure. So the SPV intensity of complex **2** is lower than that of complex **1**. Complex **3** is a mononuclear complex and the molecule is further connected to a 3D structure by hydrogen bonds and weak interactions. Hydrogen bonds belong to the class of weak bonds and they are not as capable

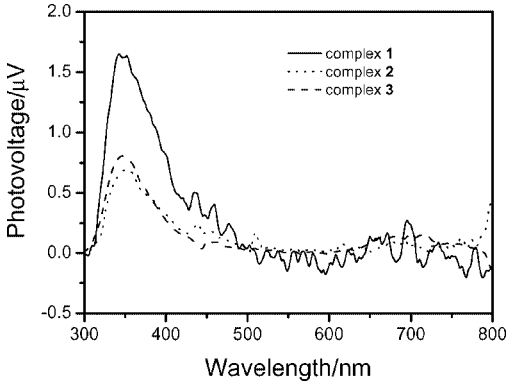

Figure 15. The contrastive SPS diagram of complexes **1**–**3**.

 © 2007 Wiley-VCH Verlag GmbH & Co. KGaA, Weinheim

in transferring electrons and holes as coordination bonds. So the SPV intensity of complex **3** is lower than that in complex **1**. Meanwhile, the 2D structure of the *ab* and *bc* planes in complex **3** are all regular structures, which benefits to the transmission of electrons and holes. Thereby, the SPV intensity of complex **3** and complex **2** is nearly the same.

FISPS of Complexes 1–3

FISPS can determine the direction of the built-in field and the mobile direction of photogeneration carriers. If we apply a positive electric field (the illuminated surface is positive) vertically to the *p*-type semiconductor surface, whose direction is the same as the direction of the built-in field, the separation efficiency of the photogeneration carriers are increased and the intensity of the SPV response increases in the original direction. If a negative electric field, whose direction is opposite to that of the built-in field, is applied, the separation efficiency of the photogenerated carriers reduces and the intensity of the SPV response is weakened, even in the reverse direction. In contrast to *p*-type semiconductors, the SPV response intensity of the *n*-type semiconductors increase as a negative field is applied and reduces as a positive electric field is applied. The FISPSs of complexes **1**–**3** are given in Figures 16, 17, and 18. The SPV responses in the range 300–800 nm in all three complexes increase linearly with a positive electric field, which shows that the direction of the positive electric field is consistent with the built-in field. This enhances the separation efficiency of the photoexcited electron-hole pairs and results in an increase in the surface potential; thus, the fact that complexes **1**–**3** have *p*-type semiconductor characteristics is confirmed. Otherwise, in complexes **1** and **2**, when adding a DC +2 V, some new SPV responses are produced: λ_{max} = 442, 490 nm for complex **1** and λ_{max} = 388, 454 nm and λ_{max} = 700 nm for complex **2**. These new SPV response bands may be attributed to the forbidden spectroscopic term transition because the external positive electric field provides more impetus for electronic transitions, which makes the forbidden transitions take place.

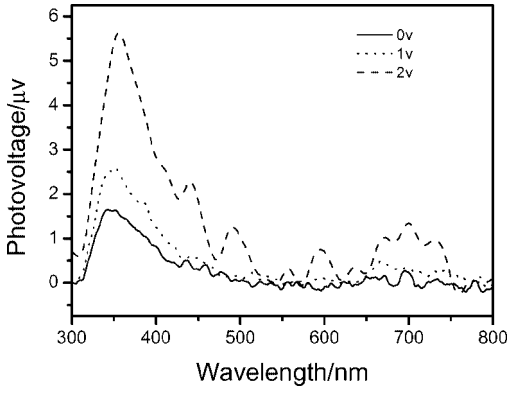

Figure 16. The FISPS of complex **1**. The intensities of the SPV response increase linearly with the external positive electric field.

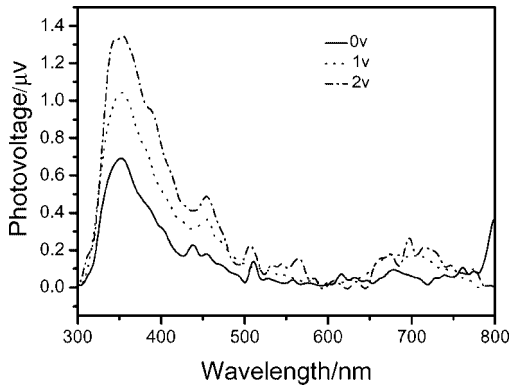

Figure 17. The FISPS of complex **2**. The intensities of the SPV response increase linearly with the external positive electric field.

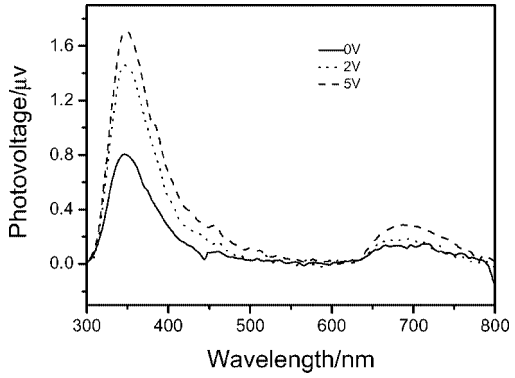

Figure 18. The FISPS of complex **3**. The intensities of the SPV response increase linearly with the external positive electric field.

Conclusion

In this paper, three Mn^{II} coordination supramolecules were synthesized by a hydrothermal method. Complex **1** possesses a 3D infinite structure. Complex **2** contains a 1D coordination chain, and the chains are further connected to a 2D infinite structure by hydrogen bonds. The 3D structure of complex **3** is completely formed by hydrogen bonds and weak interactions. The SPS of complexes **1**–**3** indicate that they all show positive SPV responses in the range 300–800 nm and all show *p*-type semiconductor characteristics. The intensities of the SPV response band at 300–500 nm in complex **1** is obviously stronger than that in complexes **2** and **3**. The differences in the intensities are attributed to the differences in their structures. The 3D structure of complex **1** is connected completely by coordination bonds and the *ab* and *bc* planes are all of regular structure. This structure style is very beneficial to the transferring of electrons and holes. Meanwhile, the microenvironment (crystal field) of the Mn^{II} ion in the complexes has a certain effect on the SPV responses, especially the d→d* transition response. Due to the crystal field, complex **2** shows a stronger response than complexes **1** and **3**, and the SPV response from the d→d* transitions are obviously different. Moreover, the FISPS confirm the *p*-type semiconductor characteristic of complexes **1**–**3**.

 © 2007 Wiley-VCH Verlag GmbH & Co. KGaA, Weinheim

Experimental Section

Materials and Methods: All the reagents are A.R grade. IR spectra were recorded in the range 220–4000 cm^{-1} with a JASCO FT/IR 480 spectrophotometer using KBr pellets. The elemental compositions of the complexes were determined with a PE-240C Analyzer and a PLASAM-SPEC-II instrument. The SPS and FISPS instrument was made by ourselves. Monochromatic light was obtained by passing light from a 500W xenon lamp through a double-prism monochromator. The slit width of the entrance and exit was 3 mm. A lock-in amplifier, synchronized with a light chopper, was employed to amplify the photovoltage signal. The range of modulating frequency is from 20 to 70 Hz. The spectral resolution is 1 nm. The samples were rubbed to power and were pressed between two slices of ITO glass during the SPS and FISPS measurements. The construction of the photovoltaic cell is an ITO/sample/ITO sandwich structure.[22] It was ensured that the light penetrating depth was much less than the powder layer thickness. All the measurements were performed under atmospheric pressure and at ambient temperature.

$[Mn(pdc)(H_2O)]_n$ (1): A solution of $MnCl_2{\cdot}4H_2O$ (0.10 g, 0.5 mmol) in water (10 mL) was added to the solution of H_2pdc(0.08 g,0.5 mmol) and NaOH (0.04 g,1 mmol) in water (10 mL); the solution was colorless. Then, this solution was transferred into a Teflon-lined stainless steel vessel, and the vessel was sealed and heated to 150 °C for 5 d. The mixture was cooled to room temp., and pink crystals of complex **1** were collected. $C_7H_5MnNO_5$ (238.06): calcd. C 35.31, H 2.12, N 5.89, Mn 23.08; found C 35.55, H 2.34, N 5.97, Mn 22.93. IR(KBr): $\tilde{\nu}$ = 3440, 3354

Table 1. Crystallographic data and structural refinement details for complexes **1**–**3**.

Complex	**1**	**2**	**3**
Empirical formula	$C_7H_5MnNO_5$	$C_{19}H_{19}MnN_3O_8$	$C_{12}H_{20}Cl_2MnN_{12}O_{16}$
M	238.06	472.31	714.24
T / K	293(2)	293(2)	293(2)
λ / Å	0.71073	0.71073	0.71073
Crystal system	monoclinic	monoclinic	monoclinic
Space group	$P2_1/c$	$P2_1/n$	$C2/m$
a / Å	6.412(3)	13.302(3)	11.786(4)
b / Å	10.785(5)	7.6274(19)	16.064(5)
c / Å	11.122(5)	19.510(5)	7.027(2)
β / °	94.760(5)	91.166(3)	116.932(4)
V / Å^3	766.5(6)	1979.2(8)	1186.1(7)
Z	4	4	2
$D_{calcd.}$ / g cm^{-3}	2.063	1.585	1.994
F (000)	476	972	722
Goodness-of-fit on F^2	1.066	1.008	1.060
Final R indices [$I > 2\sigma(I)$]	R_1 = 0.0275, wR_2 = 0.0754	R_1 = 0.0351, wR_2 = 0.0854	R_1 = 0.0629, wR_2 = 0.1687
R indices (all data)	R_1 = 0.0300, wR_2 = 0.0772	R_1 = 0.0529, wR_2 = 0.0932	R_1 = 0.0802, wR_2 = 0.1821
Data/restraints/parameters	1886/0/139	4858/8/356	1502/0/107

Table 2. Selected bond lengths [Å] and angles [°] for **1**–**3**.

1					
Mn1–O3	2.1464(16)	Mn1–O5	2.1621(16)	Mn1–O4	2.2436(18)
Mn1–O2	2.1599(17)	Mn1–O1	2.1669(17)	Mn1–N1	2.287(2)
O3–Mn1–O2	166.25(6)	O5–Mn1–O1	173.06(5)	O3–Mn1–N1	101.13(6)
O3–Mn1–O5	88.35(6)	O3–Mn1–O4	84.52(6)	O2–Mn1–N1	92.38(5)
O2–Mn1–O5	86.44(6)	O2–Mn1–O4	82.40(5)	O5–Mn1–N1	101.40(5)
O3–Mn1–O1	96.79(6)	O5–Mn1–O4	85.54(6)	O1–Mn1–N1	73.10(5)
O2–Mn1–O1	89.54(6)	O1–Mn1–O4	99.54(6)	O4–Mn1–N1	171.09(5)
2					
Mn1–O4	2.0963(13)	Mn1–O3	2.1710(13)	Mn1–N2	2.2852(15)
Mn1–O1	2.1586(15)	Mn1–N1	2.2718(16)	Mn1–N3	2.3149(15)
O4–Mn1–O1	85.37(6)	O3–Mn1–N1	90.65(6)	O4–Mn1–N3	95.75(5)
O4–Mn1–O3	111.77(6)	O4–Mn1–N2	90.21(6)	O1–Mn1–N3	158.72(6)
O1–Mn1–O3	87.94(6)	O1–Mn1–N2	115.34(6)	O3–Mn1–N3	71.87(5)
O4–Mn1–N1	155.94(6)	O3–Mn1–N2	149.74(5)	N1–Mn1–N3	99.64(5)
O1–Mn1–N1	86.90(6)	N1–Mn1–N2	72.67(6)	N2–Mn1–N3	85.92(5)
3					
Mn1–O3	2.228(4)	Mn1–O6[a]	2.238(3)	Mn1–N1	2.261(4)
Mn1–O3[a]	2.228(4)	Mn1–O6	2.238(3)	Mn1–N1[a]	2.261(4)
O3–Mn1–O3[a]	180.0	O6[a]–Mn1–O6	180.0	O3–Mn1–N1[a]	90.0
O3–Mn1–O6[a]	84.68(14)	O3–Mn1–N1	90.0	O3[a]–Mn1–N1[a]	90.0
O3[a]–Mn1–O6[a]	95.32(14)	O3[a]–Mn1–N1	90.0	O6[a]–Mn1–N1[a]	90.0
O3–Mn1–O6	95.32(14)	O6[a]–Mn1–N1	90.0	O6–Mn1–N1[a]	90.0
O3[a]–Mn1–O6	84.68(14)	O6–Mn1–N1	90.0	N1–Mn1–N1[a]	180.0

[a] Symmetry transformations used to generate equivalent atoms: –x, y, –z.

 © 2007 Wiley-VCH Verlag GmbH & Co. KGaA, Weinheim

υ(OH), 3077 υ(ArC-H), 1614 υ(asCOO), 1393 υ(sCOO), 1574, 1456 υ(ArC···C), 1241 υ(C-N), 1153, 1104 υ(C-C,C-O), 877, 844, 832, 784, 709, 659 δ(ArC-H), 455 υ(Mn-N), 429, 370 υ(Mn-O) cm^{-1}.

{[Mn(pdc) (phen)(H_2O)]·3H_2O}$_n$ (2): A solution of $MnCl_2·4H_2O$ (0.10 g, 0.5 mmol) in water (10 mL) was added to a solution of H_2pdc(0.08 g,0.5 mmol) and NaOH (0.04 g,1 mmol) in water (10 mL). An ethanol (5 mL) solution of phen (0.04 g) was then added to the above solution. The solution was yellow and clear. Then the solution was transferred into a Teflon-lined stainless steel vessel, and the vessel was sealed and heated to 170 °C for 6 d. The mixture was cooled to room temp., and pink crystals of complex **2** were collected. $C_{19}H_{19}MnN_3O_8$ (472.31): calcd. C 48.31, H 4.05, N 8.90, Mn 11.63; found C 48.52, H 4.21, N 9.12, Mn 11.49. IR (KBr): $\tilde{\nu}$ = 3395 υ(OH), 3060 υ(ArC-H), 1657 υ(asCOO), 1372 υ(sCOO), 1595, 1572, 1517, υ(ArC···C), 1233 υ(C-N), 1146, 1102 υ(C-C,C-O), 844, 726 δ(ArC-H), 444 υ(Mn-N), 420 υ(Mn-O) cm^{-1}.

{[Mn(cyan)$_2$(H_2O)$_4$]·2HCl·2(Hcyan)} (3): A solution of $MnCl_2·4H_2O$ (0.20 g, 1 mmol) in water (10 mL) was added to a solution of Hcyan (0.13 g,1 mmol) and NaOH (0.04 g,1 mmol) in water (20 mL), and the DMF (5 mL) was added into the above solution. The solution was white and muddy. The solution was then transferred into a Teflon-lined stainless steel vessel, and the vessel was sealed and heated to 100 °C for 5 d. The mixture was cooled to room temp., and colorless crystals of complex **3** were collected. $C_{12}H_{20}Cl_2MnN_{12}O_{16}$ (714.24): calcd. C 20.18, H 2.82, N 23.54, Mn 7.69; found C 20.31, H 2.85, N 23.72, Mn 7.57. IR (KBr): $\tilde{\nu}$ = 3177, 3091 υ(NH), 2992, 2852, υ(OH), 1737, 1625 υ(C=O), 1476 δ(NH), 1399 δ(OH), 1238, 1081, 993 υ(C-N, C-O), 777 υ(Cl-H), 556 υ(Mn-N), 428 υ(Mn-O) cm^{-1}.

X-ray Crystallographic Data: Crystallographic data for complexes **1**–**3** were collected with a Smart 1000 APEX II CCD diffractometer using graphite monochromated Mo-K_α radiation. (λ = 0.71073 Å) at 293 K. All data were corrected for L-P factor and empirical absorption. The structures were solved by direct methods and refined by full-matrix least-squares calculations on F^2 using the SHELXTL 97 program. All non-hydrogen atoms were refined anisotropically. Hydrogen atoms were found by mixed methods. The crystal data and structure refinement of complexes **1**–**3** are summarized in Table 1. Selected bond lengths and bond angles of complexes **1**–**3** are listed in Table 2.

CCDC-634132 (for **1**), -634133 (for **2**), and -634134 (for **3**) contain the supplementary crystallographic data for this paper. These data can be obtained free of charge from The Cambridge Crystallographic Data Centre via www.ccdc.cam.ac.uk/data_request/cif.

Supporting Information (see footnote on the first page of this article): Two correlated structure figures of complexes **1** and **2**, IR spectra of complexes **1**–**3**, principle of the SPS, analysis of the transition assignment, and equipment of the SPV technique.

Acknowledgments

This work was supported by the National Natural Science Foundation of China (Nos.20571037 and 90201018).

[1] J. Fan, L. Gan, H. Kawaguchi, W. Y. Sun, K. B. Yu, W. X. Tang, *Chem. Eur. J.* **2003**, *9*, 3965–3973.
[2] M. L. Tong, J. Wang, S. Hu, *J. Solid State Chem.* **2005**, *178*, 1518–1525.
[3] W. Dong, Q. L. Wang, S. F. Si, D. Z. Liao, Z. H. Jiang, S. P. Yan, P. Cheng, *Inorg. Chem. Commun.* **2003**, *6*, 873–876.
[4] C. Genre, G. S. Matouzenko, E. Jeanneau, D. Lunean, *New J. Chem.* **2006**, *30*, 1669–1674.
[5] X. H. Bu, M. L. Tong, Y. B. Xie, J. R. Li, H. C. Chang, S. Kitagawa, J. Ribas, *Inorg. Chem.* **2005**, *44*, 9837–9846.
[6] M. F. Anderlund, J. Högblom, W. Shi, P. Huang, L. Eriksson, H. Weihe, S. Styring, B. Åkermark, R. Lomoth, A. Magnuson, *Eur. J. Inorg. Chem.* **2006**, *24*, 5033–5047.
[7] V. L. Pecoraro (Ed.), *Manganese Redox Enzymes*, VCH, New York, **1992**.
[8] M. Fujiware, T. Matsushita, S. Ikeda, *J. Electron. Spectrosc. Relat. Phenom.* **1995**, *74*, 201–206.
[9] S. Ohkoshi, H. Tokoro, M. Utsunomiya, M. Mizuno, M. Abe, K. Hashimoto, *J. Phys. Chem. B* **2002**, *106*, 2423–2425.
[10] D. Dobraynska, L. B. Jeraykiewicz, J. Jezierska, M. Duczmal, *Cryst. Growth Des.* **2005**, *5*, 1945–1951.
[11] A. Murphy, G. Dubois, T. D. P. Stack, *J. Am. Chem. Soc.* **2003**, *125*, 5250–5251.
[12] X. H. Liu, M. Krott, P. Műller, C. H. Hu, H. Lueken, R. Dronskowski, *Inorg. Chem.* **2005**, *44*, 3001–3003.
[13] D. Ghoshal, A. K. Ghosh, J. Ribas, E. Zangrando, G. Mostafa, T. K. Maji, N. R. Chaudhuri, *Cryst. Growth Des.* **2005**, *5*, 941–947.
[14] J. F. Chai, H. P. Zhu, A. C. Stűckl, H. W. Roesky, J. Magull, A. Bencini, A. Caneschi, D. Gratteschi, *J. Am. Chem. Soc.* **2005**, *127*, 9201–9206.
[15] D. J. Wang, J. Zhang, T. S. Shi, B. H. Wang, X. Z. Cao, T. J. Li, *J. Photochem. Photobiol. A* **1996**, *93*, 21–25.
[16] Q. L. Zhang, D. J. Wang, J. J. Xu, J. Cao, J. Z. Sun, M. Wang, *Mater. Chem. Phys.* **2003**, *82*, 525–528.
[17] L. P. Sun, S. Y. Niu, J. Jin, G. D. Yang, L. Ye, *Eur. J. Inorg. Chem.* **2006**, 5130–5137.
[18] T. F. Xie, D. J. Wang, L. J. Zhu, C. Wang, T. J. Li, *J. Phys. Chem. B* **2000**, *104*, 8177–8181.
[19] A. Kokler, J. Gruner, R. H. Friend, K. Mullen, V. Scherf, *Chem. Phys. Lett.* **1995**, *243*, 456–461.
[20] J. Zhang, D. J. Wang, T. S. Shi, B. H. Wang, J. Z. Sun, T. J. Li, *Thin Solid Films* **1996**, *284/285*, 596–599.
[21] H. F. Mao, H. J. Tian, Q. F. Hou, H. J. Xu, *Thin Solid Films* **1997**, *300*, 208–212.
[22] K. Y. Li, D. J. Wang, F. Q. Wu, T. F. Xie, T. J. Li, *Mater. Chem. Phys.* **1999**, *60*, 226–230.

Received: February 13, 2007
Published Online: June 29, 2007

 © 2007 Wiley-VCH Verlag GmbH & Co. KGaA, Weinheim